Influence of y' precipitate-size and distribution on LCF behavior of a PM disk superalloy

Guylaine Boittin, D. Locq, A. Rafray, P. Caron, Pascale Kanoute, F. Gallerneau, Georges Cailletaud

Superalloys 2012: 12th International Symposium on Superalloys
Edited by: Eric S. Huron, Roger C. Reed, Mark C. Hardy, Michael J. Mills, Rick E. Montero, Pedro D. Portella, Jack Telesman
TMS (The Minerals, Metals & Materials Society), 2012

INFLUENCE OF γ' PRECIPITATE SIZE AND DISTRIBUTION ON LCF BEHAVIOR OF A PM DISK SUPERALLOY

G. Boittin[1], D. Locq[1], A. Rafray[1], P. Caron[1], P. Kanouté[1], F. Gallerneau[1] and G. Cailletaud[2]
[1]Onera – The French Aerospace Lab, F-92322 Châtillon, France
[2]Centre des Matériaux, Mines ParisTech, CNRS UMR 7633, F-91003 Evry, France

Keywords: disk superalloy, powder metallurgy, γ' precipitation, tensile properties, LCF, mean stress, modeling, CRSS

Abstract

The influence of γ' precipitate distribution on tensile and low cycle fatigue (LCF) behaviors of a powder metallurgy (PM) disk superalloy was investigated at 450°C. Four γ' particle distributions were obtained through various cooling paths and/or aging treatments in coarse grain size superalloy N18. The mechanical tests show that the main influence of the intragranular microstructure concerns the 0.2% yield stress (0.2%YS) and the ultimate tensile stress. Wide variations of the 0.2%YS affect the mean stress under non symmetrical loading but have only little effect on fatigue life, the lower the 0.2%YS, the longer the fatigue life. The fatigue life of N18 at 450°C is independent of the intragranular microstructure as long as the mean stress effect is correctly taken into account. As expected with the coarse grain size N18, no crack initiation at pores or inclusions was observed.

A precipitation model was coupled with a critical resolved shear stress calculation providing 0.2%YS value for a given heat treatment sequence. Finally, this computation procedure was implemented in a numerical modeling of the LCF life of a disk taking into account the heat treatment applied to its wrought preform.

Introduction

The service life of aeroengine high-pressure disks is highly dependent on their low cycle fatigue (LCF) resistance at low and intermediate temperatures. Polycrystalline γ/γ' nickel-based wrought superalloys are commonly used for the last high-pressure compressor (HPC) stages and for the low and high-pressure turbine (LPT and HPT) disks.

Little data exists for alloys like N18 regarding the microstructural influence on LCF properties as compared with those concerning the effect of the microstructure on their tensile or creep behavior. This is partly due to the high cost and complexity of LCF tests, and the commercial value of this kind of data precludes their dissemination. These LCF tests could have long duration and numerous tests are needed to properly account for data scatter. Finally, a higher number of testing parameters (as load or strain control, minimum/maximum load (or strain) ratio, frequency…) makes the comparison of fatigue data more difficult than for tensile or creep results.

Effect of the grain size was widely studied and, in most cases, the larger the grain size, the shorter the fatigue life [1-10]. But only a limited number of studies were devoted to the influence of the γ/γ' microstructure on the LCF behavior of these materials. For instance, the longest lives were obtained for the heat treatment leading to the most homogeneous deformation and the lowest maximum stress during a fatigue cycle for alloy René 95 [11]. The corresponding microstructure is characterized by the coarsest secondary γ' precipitate size and no tertiary γ' particles (982°C/72h aging) but also by the finest grain size. Changes in the γ' precipitate size and distribution frequently occur together with grain size variations that makes difficult the analysis of the microstructural effects. A computational study can get around this issue and provide qualitative trends. Such an approach applied to the IN100 alloy with virtual microstructures showed that the maximum fatigue crack initiation life at 650°C was reached with the smallest secondary γ' fraction and size associated with the largest tertiary γ' fraction and size (within the investigated ranges) [12].

However, the effects of the strengthening γ' precipitate size and distribution on LCF resistance were unfortunately often masked due to crack nucleation events at defects resulting from the processing route such as carbonitrides for cast and wrought superalloys [5] or pores and ceramic inclusions for powder metallurgy (PM) superalloys [13]. This trend is almost systematically observed in fine grain size materials. For coarser grain size superalloys (typically when the grain size is larger than the ceramic inclusions), depending on the LCF conditions, cracks initiate preferentially at a crystallographic facet [2, 4, 7, 12]. Furthermore, the crack initiation mechanism depends not only on grain size but also on LCF test conditions such as the temperature [2], the strain amplitude [14, 15] or the strain ratio [16].

The aim of the present study is therefore to analyze the influence of γ' precipitate distribution on the tensile and LCF behaviors of a disk superalloy. To promote crack nucleation at intense slip bands (leading to crystallographic facets), this work was carried out on a coarse grain size material.

Material

This work was performed on PM superalloy N18 [17]. This superalloy is used for the production of the disks of the last HPC stages and of the HPT of the M88 Snecma engine. Disk parts were processed and provided by Snecma in the extruded and isoforged state. Table I provides the composition of the N18 batch used for this study.

Table I. Composition of the N18 superalloy in wt%

Ni	Co	Cr	Mo	Al	Ti	Hf
Bal.	15.40	11.25	6.50	4.42	4.35	0.48
		B	**C**	**Zr**		
		0.016	0.016	0.028		

The γ' fraction of this alloy is about 55-60%, its γ' solvus temperature is around 1195°C and its density is 8 $g \cdot cm^{-3}$. After forging, the typical microstructure of the N18 alloy consists of a very fine grain size (2-3 µm) due to a high fraction of primary γ'

phase (25 to 30 % of coarse γ' particles are not solutionized during the subsolvus extrusion and forging processes).

Production of N18 powder by argon atomization inevitably leads to the presence of ceramic inclusions in the forged parts. N18 powders are sieved at 53 µm (-270 mesh) to use fine superalloy powders and to minimize the number and size of the ceramic particles. As these inclusions are brittle and are preferred sites for crack initiation when their size is greater than the grain size, they are deleterious for LCF resistance. Their impact depends on their brittleness, shape, location and size.

In subsolvus heat treated N18 where coarse primary γ' particles prevent grain growth, grain sizes remain within the range of 10-15 µm. During LCF tests, cracks mostly initiate from ceramic inclusions larger than the grains. In supersolvus heat treated N18 with coarse grains (40-60 µm), the size of the inclusions is smaller or of the same order as the grain size, and most of the cracks initiate from a crystallographic plane. It is therefore easier to investigate the effect of the intragranular microstructure on LCF behavior in coarse grain material than in fine grain alloy where crack initiation from inclusions would mask this effect. Moreover crack initiation on inclusion leads to a wide dispersion in the fatigue life results. Indeed, the inclusions are randomly distributed in the material, so it is impossible to predict if one inclusion is at the critical point, if so, the life is shortened. This problem should not occur in the coarse grain microstructure, as it is likely to find a coarse grain favorably oriented for crack initiation near the critical point.

Microstructures

Cylindrical rods (Ø12 mm x 58 mm) were extracted by electrical-discharge machining from as-forged disks and were then individually heat treated. The grain size was estimated by comparison of optical micrographs to a series of graded images. Secondary γ' precipitate size was determined by image analysis (IA) of pictures acquired by scanning electron microscopy (SEM-FEG Zeiss DSM982 GEMINI) on an etched specimen. The image analysis was carried out on 300 to 600 precipitates and the secondary γ' precipitate size in Table II is taken as the mean edge of these particles considering an almost cubical shape. The tertiary γ' precipitate size is an estimate of the mean diameter (spherical particles) deduced from both "SEM+IA" and manual measurements on transmission electron microscopy (TEM) dark field images.

The four supersolvus microstructures investigated in this study are characterized by an identical coarse grain size resulting from a supersolvus heat treatment for two hours at 1200°C. This heat treatment eliminates all the primary γ' particles enabling grain growth up to about 50 µm. The microstructural variations (γ' precipitate distribution) were obtained through various cooling paths and/or aging treatments.

The "reference" microstructure is obtained through a supersolvus heat treatment (1200°C/2h) ended by air cooling (AC), followed by a double aging treatment for 24 hours at 700°C, then for 4 hours at 800°C. This heat treatment leads to a bimodal γ' particle size distribution (Figure 1a): secondary γ' precipitates with a cubical shape and a mean edge of about 165 nm and spherical tertiary γ' precipitates with a mean diameter close to 25 nm.

The "no γ'_{III}" (no tertiary γ' precipitates) microstructure results also from a supersolvus heat treatment (1200°C/2h) ended by air cooling. But to eliminate the tertiary γ' population which precipitates during the last stage of the air cooling, an aging treatment of one hour at 900°C was then applied. A slight increase of the secondary γ' size is measured (Table II) and coalesced tertiary γ' precipitates are sparsely observed in between the secondary particles (Figure 1b). As N18 superalloy is prone to topologically closed packed (TCP) phases (identified as σ and µ phases [18]), fine intergranular precipitates were noticed at very few grain boundaries. It is assumed that this small amount of TCP phase particles has no significant influence on the mechanical behavior.

The "fine γ'_{II}" (fine secondary γ' precipitates) microstructure is obtained after a supersolvus heat treatment (1200°C/2h) followed by water quenching (WQ) and the same double aging treatment as for the "reference" microstructure. The higher cooling rate leads to a smaller mean size of the secondary γ' precipitates (≈ 115 nm) and the double aging treatment produces the same tertiary γ' diameter (≈ 25 nm) as compared with the "reference" microstructure (Figure 1c).

The fourth microstructure is designated as "coarse γ'_{II}" (coarse secondary γ' precipitates) and results from the following heat treatment procedure:

- 1200°C/2h followed by a slow cooling rate of 4°C/min down to 1000°C then continued by a slow cooling rate of 1°C/min down to 900°C and then air cooled,
- 700°C/24h/AC.

Table II. Heat treatments applied to N18 alloy and resulting experimental and calculated microstructural data

			Experimental measurements		Calculation
Microstructure designation	Solution heat treatment	Aging treatment	γ'_{II} mean edge (nm)	γ'_{III} mean diameter (nm)	γ'_{II} mean edge (nm)
"reference"	1200°C/2h/AC	700°C/24h/AC + 800°C/4h/AC	164	25	201
"no γ'_{III}"	1200°C/2h/AC	900°C/1h/AC	174	-	206
"fine γ'_{II}"	1200°C/2h/WQ	700°C/24h/AC + 800°C/4h/AC	113	25	124
"coarse γ'_{II}"	1200°C/2h/4°C·min^{-1} cooling → 1000°C then 1°C·min^{-1} cooling → 900°C/AC	700°C/24h/AC	1000-4000	-	1450

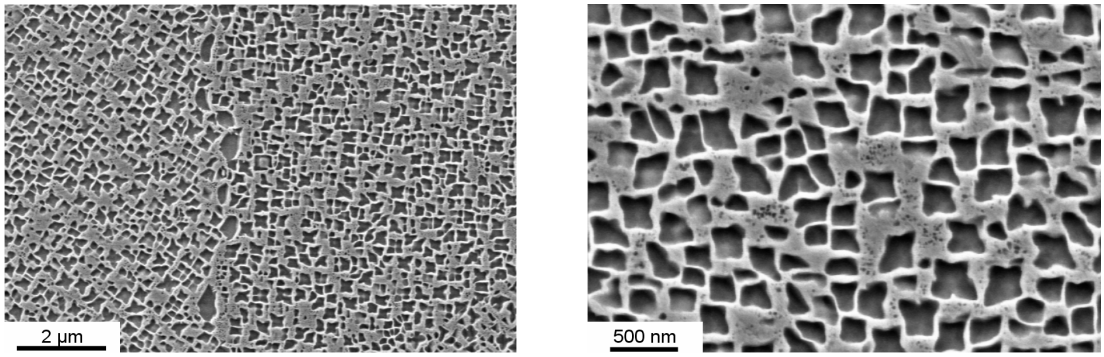

a) "reference" microstructure (1200°C/2h/AC + 700°C/24h/AC + 800°C/4h/AC)

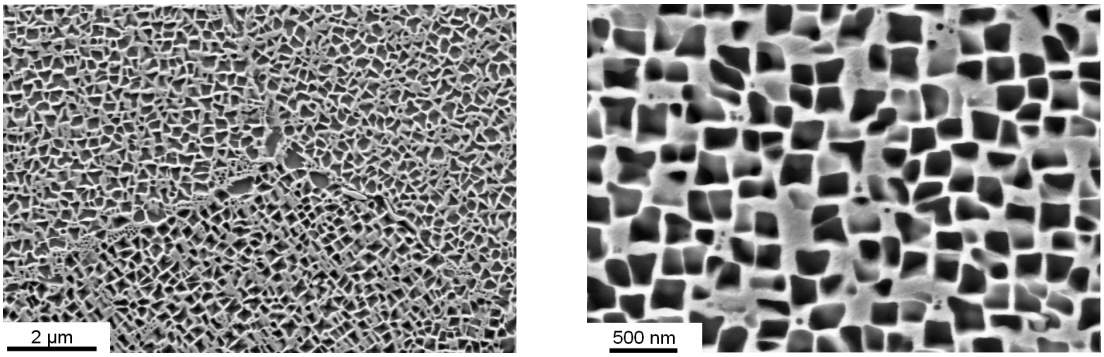

b) "no γ'_{III}" microstructure (1200°C/2h/AC + 900°C/1h/AC)

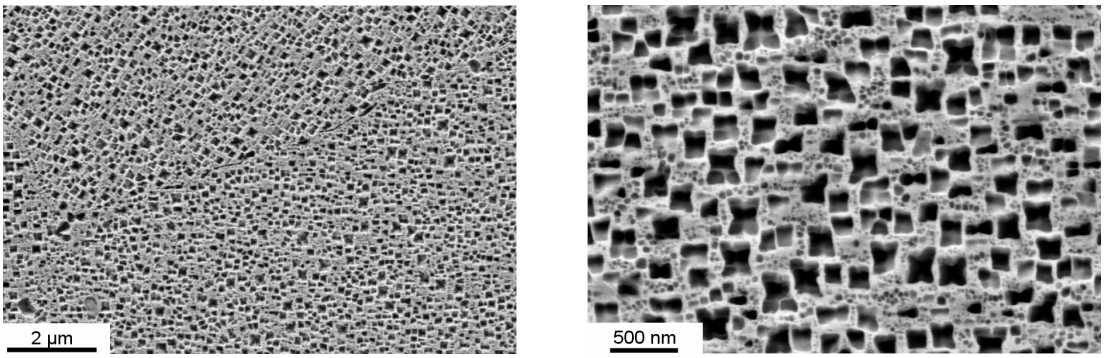

c) "fine γ'_{II}" microstructure (1200°C/2h/WQ + 700°C/24h/AC + 800°C/4h/AC)

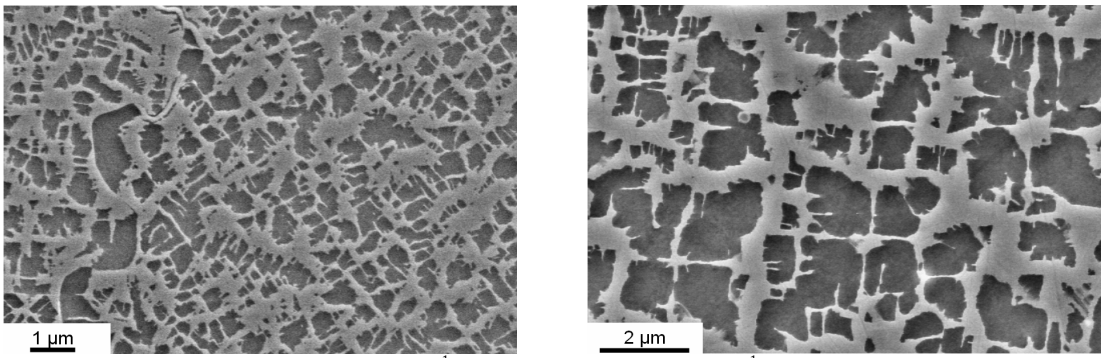

d) "coarse γ'_{II}" microstructure (1200°C/2h/4°C·min^{-1} cooling → 1000°C then 1°C·min^{-1} cooling → 900°C/AC + 700°C/24h/AC)

Figure 1. Microstructures of supersolvus N18 after various heat treatment sequences.
Lower magnifications are used for the "coarse γ'_{II}" microstructure (SEM-secondary electron mode-etched specimens).

This heat treatment procedure generates a very coarse γ′ precipitation (Figure 1d). The first slow cooling induces nucleation of a limited number of precipitates which can growth during the long cooling duration. The second slow cooling is carried out to prevent further γ′ particle nucleation and to promote the growth of the present precipitates. The aging treatment was applied to ensure that no tertiary γ′ precipitation occurs. The SEM images show that the coarse γ′ precipitates tend to grow along preferential directions and to split. As expected, this phenomenon is accompanied by the formation of serrated grain boundaries [19]. No image analysis was undertaken on such a messy microstructure but the edge of these coarse secondary γ′ precipitate was manually measured to be between 1-4 micrometers. No or very few tertiary γ′ precipitates are observed within the wide γ channels (Figure 1d).

These four microstructures were designed to achieve very distinct tensile behaviors and to study the influence of the two populations of γ′ precipitates on LCF resistance. Finally, the precipitation parameters of the first three microstructures and of other N18 microstructures were used as data to recalibrate and validate a precipitation model previously developed for the subsolvus N18 (presence of primary γ′ precipitates) [20, 21]. This model allows the calculation of the volume fraction and the mean size of each population of γ′ precipitates [22]. Only the calculated mean edges of the secondary γ′ precipitates are included in Table 1. They are shown to be in good agreement with the experimental measurements except for the "coarse γ'_{II}" microstructure for which the microstructural data were not accurately determined and the model is consequently not suitable.

Mechanical characterization

Test matrix

Mechanical tests were conducted at 450°C in air on smooth specimens with 14 mm length x 4.4 mm diameter gage dimensions. The five mechanical tests performed for each microstructure are presented in Table III.

Table III. Mechanical test parameters

Test designation	Test conditions
Tensile	strain rate of $10^{-3}s^{-1}$
Repeated LCF	$R\varepsilon = 0$, $\Delta\varepsilon/2 = 0.35\%$ strain rate of $10^{-3}s^{-1}$(triangular waveform)
	$R\varepsilon = 0$, $\Delta\varepsilon/2 = 0.45\%$ strain rate of $10^{-3}s^{-1}$(triangular waveform)
	$R\varepsilon = 0.6$, $\Delta\varepsilon/2 = 0.2\%$* 15 Hz (sinusoidal waveform)
Fully reversed incremental LCF	$R\varepsilon = -1$, strain increments strain rate of $10^{-3}s^{-1}$(triangular waveform)

* During this test, only the first cycle was conducted under strain control, the other cycles were under stress control between two stress levels corresponding to a strain cycling between 0.6% and 1%.

The strain ratio $R\varepsilon$ is defined as $\varepsilon_{min}/\varepsilon_{max}$ and the strain amplitude $\Delta\varepsilon/2$ is defined as $(\varepsilon_{max} - \varepsilon_{min})/2$. In the same way, the stress amplitude $\Delta\sigma/2$ is equal to $(\sigma_{max} - \sigma_{min})/2$ at the stabilized cycle.

A high pressure turbine disk experiences temperatures between 300 and 650°C during service life. The temperature of 650°C is reached only in the rim, and the disk bore undergoes lower temperature. 450°C is a representative temperature for the web of the disk. Moreover, this temperature offers the advantage to minimize the risk of crack initiation from inclusion. For SMO43 alloy (now N19 alloy), Guédou *et al.* [23] have indeed observed, that at 650°C, even with a coarse grain size, the fatigue crack may initiate from inclusions, whereas at 450°C this crack initiation mode is much less frequent.

The monotonic tensile test provides elastic modulus (E), hardening modulus, 0.2% yield stress (0.2%YS) and ultimate tensile stress (UTS). The two repeated LCF tests with $R\varepsilon = 0$, were designed to plot the mean stress curve (mean stress at the stabilized cycle as a function of imposed maximum strain). The expected fatigue lives were respectively of the order of 10^5 and 10^4 cycles for $\Delta\varepsilon/2 = 0.35\%$ and $\Delta\varepsilon/2 = 0.45\%$. The fully reversed incremental LCF test was performed to plot the cyclic hardening curve. For this test, a strain amplitude level of 0.5% was first applied during at least 300 cycles to reach the stabilized cycle and then a strain amplitude level of 0.7% was applied until the specimen rupture. For the first tested specimen ("no γ'_{III}" microstructure), a third strain level of 0.9% was tried but led to a small number of cycles to rupture (< 100) so this procedure was not applied to the following tests. For each microstructure, the fatigue life is defined as the number of cycles to rupture at the higher strain level. For these tests, the rupture occurred before 1000 cycles, i.e. in the short fatigue life regime. Finally, the repeated LCF test with $R\varepsilon = 0.6$ was designed to reach a long fatigue life of the order of 10^6 cycles. It leads to a high mean stress, more representative of the loading of a high pressure turbine disk.

Thus, despite a small number of experiments, the test matrix covers a wide fatigue life range, from 10^2 to 10^6 cycles, and allows studying some key features of the fatigue behavior, such as the mean stress relaxation and the cyclic hardening.

Experimental results

Monotonic tensile tests. Analysis of the tensile curves (Figure 2) indicates that the elastic and the hardening moduli are hardly dependent on the γ′ precipitate distribution. On the contrary, microstructural changes induce large variation of the 0.2%YS. The dissolution of the tertiary γ′ precipitates leads to a 70 MPa 0.2%YS decrease (in comparison with the "reference" microstructure). A fine secondary γ′ precipitation offers a 320 MPa advantage when compared with the coarse secondary γ′ precipitation that highlights the strong influence of the secondary γ′ precipitate size on the 0.2%YS (Table IV).

Table IV. Data of the tensile tests at 450°C

Microstructure	E (GPa)	0.2%YS (MPa)	UTS (MPa)	Elongation (%)
"fine γ'_{II}"	195 ± 7	1135	1483	16.1
"reference"		1048	1410	14.3
"no γ'_{III}"		975	1420	19.1
"coarse γ'_{II}"		812	1280	35.8

Some plastic instabilities can be observed on some tensile curves (Figure 2), especially in the case of the "reference" microstructure. These events are a drawback of the choice of the test temperature, which corresponds to the domain in which strain aging phenomena may occur. These events occur at high strain level (> 1%) and globally did not affect the results of the LCF

tests. The ultimate tensile stress (UTS) shows the same trend as the 0.2%YS except for the "reference" microstructure for which the UTS value can be related to the unexpected low ultimate elongation.

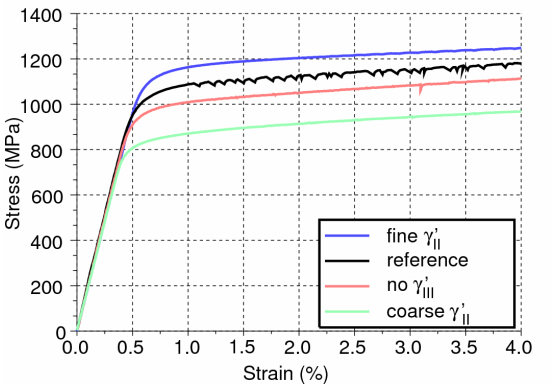

Figure 2. Tensile curves at 450°C
for supersolvus N18 with various microstructures.

Fatigue behavior. Analysis of the cyclic test results allowed the quantification of the cyclic hardening and of the mean stress at the stabilized cycle for various strain levels. The cyclic hardening amplitude and the mean stress relaxation are indeed two key parameters for the calculation of the fatigue life.

The cyclic hardening curves were drawn from different fatigue tests (Figure 3). The plastic strain amplitude represents $(\varepsilon_{plastic\ max} - \varepsilon_{plastic\ min})/2$ at the stabilized cycle. The fully reversed LCF tests conducted with several strain increments provide several points at relatively high plastic strain. A strong cyclic hardening is systematically observed. Its amplitude $(\sigma_{cyclic} - \sigma_{monotonic})$ is quite similar whatever the microstructure (about 240 MPa for a plastic strain of 0.1%). Therefore, in a first approximation, the cyclic hardening can be considered independent of the intragranular microstructure.

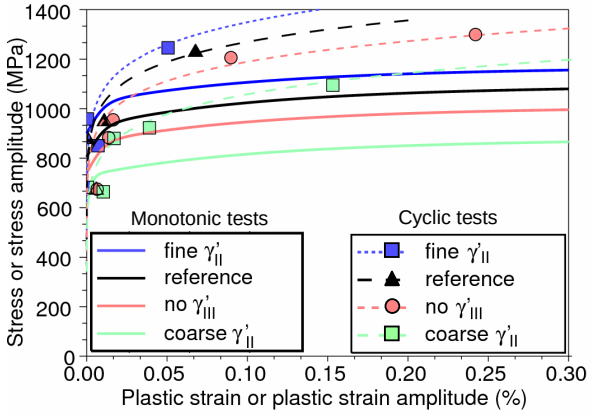

Figure 3. Cyclic hardening curves at 450°C for supersolvus N18 with various microstructures. Solid lines are the monotonic tensile curves, dots and dotted lines are cyclic hardening test results.

When plotting mean stress curve (mean stress at the stabilized cycle vs. the maximum strain) as in the Military Handbook [24], the curve can be divided in three parts. As long as the maximum stress during the stabilized cycle is below the 0.2%YS (low strain amplitude), the material behavior is considered in the following analysis to be purely elastic and the mean stress is given by:

$$\bar{\sigma} = E\Delta\varepsilon/2 \quad (1)$$

with E the elastic modulus and Δε/2 the strain amplitude. When the maximum stress is above the 0.2%YS during the stabilized cycle, the mean stress is given by:

$$\bar{\sigma} = 0.2\%YS - E\Delta\varepsilon/2 \quad (2)$$

as the material is considered to behave as perfectly plastic. For higher strain amplitudes, the mean stress becomes null.

The "elastic segment" of the curve is common to all microstructures, as their moduli are very close. However, the lessening segment, corresponding mostly to elastically adapted cycles, is different for each microstructure due to distinct 0.2%YS. Figure 4 shows that experimental results are in good agreement with these mean stress curves, evidencing that the γ' distribution strongly affects the mean stress reached at the stabilized cycle in the same way as the 0.2%YS.

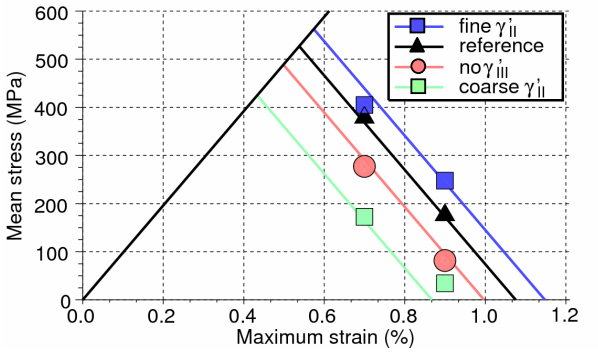

Figure 4. Mean stress relaxation curves at 450°C for supersolvus N18 with various microstructures. Equations 1 and 2 are depicted as straight lines and experimental results of repeated LCF tests with Rε = 0 as dots.

Fatigue life. As shown in Figure 5, the lower the mean stress, the longer the fatigue life. Indeed, for a repeated LCF test with a loading of Rε = 0, Δε/2 = 0.35% or Rε = 0.6, Δε/2 = 0.2%, the stabilized cycle is elastically adapted, thus the stress amplitude is equal to the imposed strain amplitude multiplied by the elastic modulus (Δσ/2 = EΔε/2), and the maximum stress is equal to the addition of the mean stress and the stress amplitude ($\sigma_{max} = \bar{\sigma} + \Delta\sigma/2$). A lower maximum stress therefore indicates a lower mean stress.

Smith, Watson and Topper (SWT) [25] proposed a model of fatigue, using an effective stress described as $\sigma_{eff} = \sqrt{E\sigma_{max}\Delta\varepsilon/2}$ with σ_{max} and Δε/2 determined at the stabilized cycle. This effective stress is plotted as a function of the number of cycles to rupture in Figure 6. Mean stress effect is taken into account in this representation as $\sigma_{max} = \bar{\sigma} + \Delta\sigma/2$, so:

$$\sigma_{eff} = \sqrt{E\frac{\Delta\varepsilon}{2}\left(\frac{\Delta\sigma}{2} + \bar{\sigma}\right)} \quad (3).$$

For all the microstructures, lifetime follows the same fatigue law. The fatigue law is therefore independent of the intragranular microstructure. However, the effect of the microstructure on the mean stress plays a role in the fatigue life, even if it is a minor one. This is particularly noticeable on fatigue life for the tests at $R\varepsilon = 0.6$, $\Delta\varepsilon/2 = 0.2\%$: for the same test conditions, samples with the different intragranular microstructures exhibit different mean stresses. As mean stress has an influence on the effective stress, this difference leads to a fatigue life ten times longer (Figure 5b).

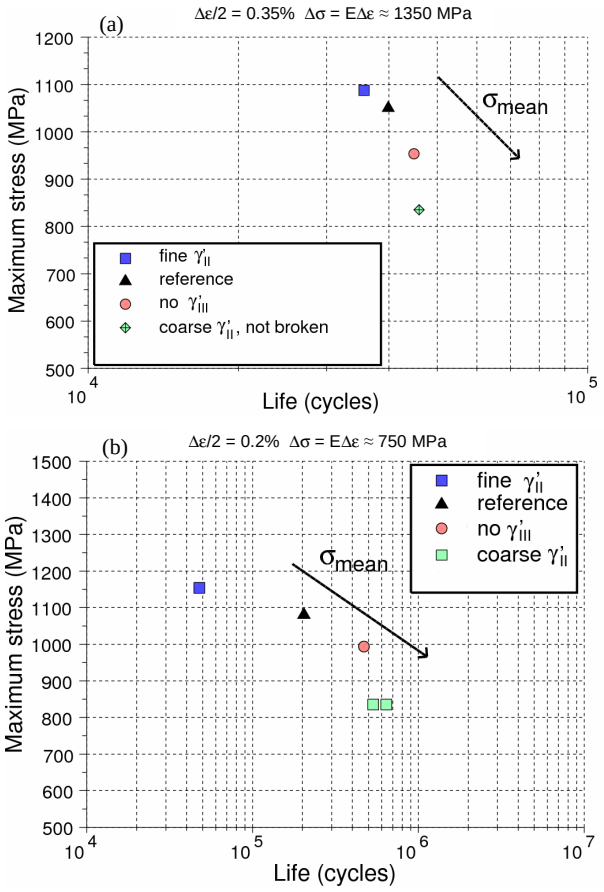

Figure 5. Mean stress effect on 450°C fatigue life of supersolvus N18 with various microstructures for two repeated LCF test conditions: (a) $R\varepsilon = 0$ and $\Delta\varepsilon/2 = 0.35\%$ and (b) $R\varepsilon = 0.6$ and $\Delta\varepsilon/2 = 0.2\%$.

The mean stress effect on the fatigue life can be also evidenced by plotting the strain amplitude as a function of the fatigue life for different strain ratio and a given microstructure. Figure 7 compares these curves for three strain ratios for the reference microstructure. Here the curves for $R\varepsilon = 0$ and $R\varepsilon = 0.6$ are derived from the curve for $R\varepsilon = -1$, taking into account the effect of the mean stress through the effective stress. The effective stress is defined using the behavior model identified by Boittin for alloy N18 [22]. The curves are superimposed for the high strain amplitude, for which the mean stress is close to zero, but are different for small strain amplitudes corresponding to elastically adapted loading.

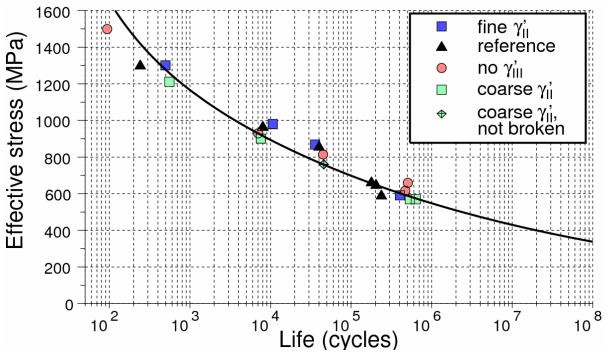

Figure 6. Fatigue life at 450°C for supersolvus N18 with various microstructures.

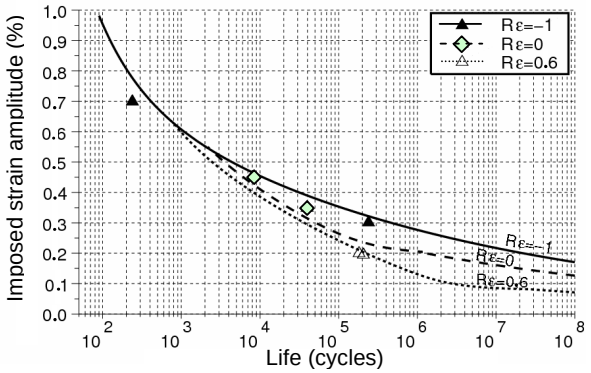

Figure 7. Fatigue life at 450°C for the "reference" microstructure of alloy N18 with various strain ratios.

For all the tested LCF conditions, the large grain size (50 µm) effectively enables to evidence effects of γ' distribution on the fatigue behavior of the superalloy N18. One major result is that although the γ' precipitate size and distribution have a strong influence on 0.2%YS and on the mean stress relaxation during cyclic tests, these microstructural parameters have only limited influence on the fatigue life of alloy N18 in the investigated range of fatigue life (typically 10^2 to 10^6 cycles).

Crack initiation. As expected, analyses of the fracture surfaces indicate that cracks never nucleate at pores or ceramic inclusions but mainly at large crystallographic facets. The orientation of these facets is close to 45° with respect to the loading axis. The fractography of the specimen with reference microstructure submitted to a repeated LCF test ($R\varepsilon = 0$, $\Delta\varepsilon/2 = 0.35\%$) shows an example of crack initiation on such a large facet (Figure 8).

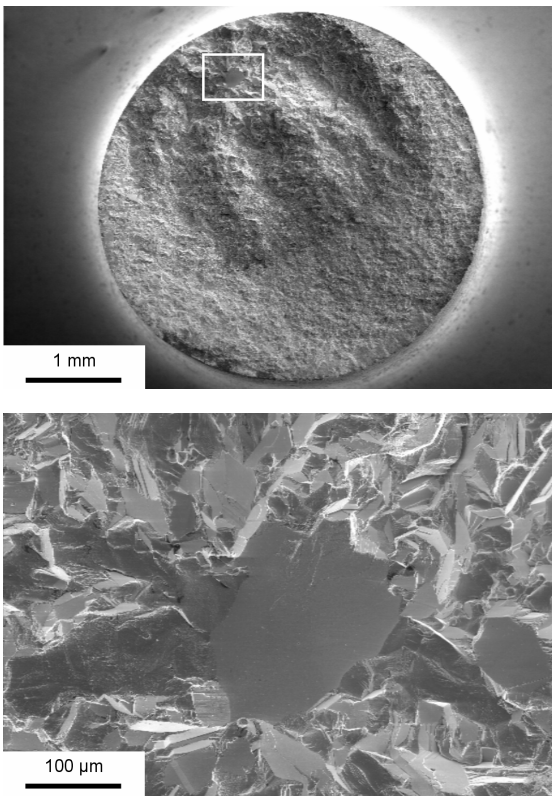

Figure 8. Fracture surface and initiation crack site of the "reference" microstructure N18 specimen tested at 450°C (LCF test with Rε = 0 and ε_{max} = 0.7%) (SEM images).

Modeling of the γ' precipitate effect on the plastic threshold

The influence of the size and volume fraction of a population of precipitates on the yield stress can be modeled considering the movement of dislocations inside and in the vicinity of the precipitates.

In face-centered cubic alloys, dense planes are {111} and dense directions are ⟨110⟩. In the disordered matrix stresses are relaxed by perfect dislocations of Burgers vector $a/2\langle 110\rangle$ (a lattice parameter of γ) gliding on {111} planes. But in $L1_2$ ordered γ' precipitates, a perfect dislocation has a Burgers vector of $a\langle 110\rangle$ because a dislocation of Burgers vector of $a/2\langle 110\rangle$ would modify the order and induce an antiphase boundary (APB). Therefore, to shear a precipitate, dislocations of the matrix are paired. If the two dislocations are both together in the same precipitate, they are strongly coupled. On the contrary, if the leading dislocation can pass entirely through a precipitate without the trailing one enters it, they are weakly coupled.

Approaches considering the resolved shear stress necessary to move a dislocation through a glide plane containing precipitates were first described:

- by Orowan, for dislocations bypassing the precipitates,
- by Hüther and Reppich [26], for strongly coupled dislocations shearing the precipitates,
- and by Brown and Ham [27], for weakly coupled dislocations shearing the precipitates.

In these models, a dislocation is considered as a flexible line with a line tension T_L moving in its glide plane and the precipitates are spherical obstacles regularly disposed, described by f the surface fraction of the precipitates, R their mean radius and Γ_{APB} the antiphase boundary energy. The critical resolved shear stress is the stress necessary to make the dislocation pairs go entirely through the glide plane.

Hüther and Reppich calculated τ_{HR} the critical resolved shear stress (CRSS) in the case of strong pair-coupling cutting of the precipitates as [26]:

$$\tau_{HR} = 0.415\frac{T_L w f^{1/2}}{bR}\left(\frac{\pi^2 R\Gamma_{APB}}{4wT_L} - 1\right)^{1/2}\left(0.94\left(1 + C_{SL}\frac{f^{1/2}}{2}\right)\right) \quad (4)$$

and τ_{SL} the CRSS in the case of weak pair-coupling cutting of the precipitates would be [28]:

$$\tau_{SL} = \frac{\Gamma_{APB}}{2b}\left(A_1\left(\frac{\Gamma_{APB} Rf}{T_L}\right)^{1/2} + A_2 f\right)(1 + C_{SL}\eta_{SL}) \quad (5)$$

with A_1 and A_2 fitting coefficients (A_1 = -A_2 = 0.75), C_{SL} an empirical constant (C_{SL} = 1 [29]) and η_{SL} is defined as $\eta_{SL} = f^{1/2}/2$ as in [29]. w is a parameter accounting for the elastic repulsion of the dislocation within the precipitate (w = 3.34 [29]). T_L is the dislocation line tension ($T_L = Gb^2/2$ with G the shear modulus (G = 80 GPa [29]) and b the Burgers vector ($b = a/\sqrt{2}$ = 0.254 nm as a = 0.3598 nm [18])). For the antiphase boundary energy, a typical value of Γ_{APB} = 0.23 J·m^{-2} was chosen [30].

For instance, for a population of precipitates with a mean radius R = 70 nm and a volume fraction of 0.50, τ_{HR} is equal to 344 MPa and τ_{SL} to 582 MPa. As $\tau_{HR} < \tau_{SL}$, the precipitates are sheared by strongly coupled dislocations and they induce a plastic threshold stress of the material of $\tau = \tau_{matrix} + \tau_{HR}$ where τ_{matrix} is the shear stress of the solid solution matrix without any precipitates. In alloy N18, there are two populations of precipitates. They are considered to have no interactions and their contributions to CRSS are simply added. Usually tertiary γ' are considered to be sheared by weakly coupled dislocations and secondary γ' by strongly coupled ones [31]. However, especially for the tertiary γ' precipitates, it would be better to systematically calculate τ_{HR} and τ_{SL} to select the right mechanism. Thus,

$$CRSS = \tau = \tau_{matrix} + \tau_{HR\,or\,SL(\gamma'_{II})} + \tau_{HR\,or\,SL(\gamma'_{III})} \quad (6).$$

The chosen value for τ_{matrix} is 85 MPa and is in good agreement with the value estimated by Espié for the nickel-based single crystal superalloy AM1 at 25 and 650°C (73 MPa [32]).

The yield stress or plastic threshold stress is calculated from the CRSS by considering that the first grains which will be plastified are the most favorably oriented ones (i.e. with the highest Schmid factor (0.5)). The yield stress is consequently two times the CRSS. A hardening of 240 MPa was observed between 0 and 0.2% strain. Thus,

$$0.2\%YS = 2\times CRSS + 240MPa \quad (7).$$

Comparison between the model (calculations with the experimental microstructure parameters or with the model microstructure parameters resulting from [22]) and the 0.2%YS measured on the tensile curve shows an excellent agreement (Table IV). This calculation was not performed for the "coarse γ'_{II}" microstructure due to the lack of reliable experimental measurements on this microstructure. The irregular shapes of the coarse γ' precipitates (figure 1d) make both the IA results and the CRSS calculations too inaccurate.

The coupling of the precipitation model and the CRSS calculation provides a good estimate of the 0.2%YS value from a given heat treatment sequence.

Modeling of the influence of heat treatment on the fatigue life of a disk

The present study is part of a project aiming at computing the influence of heat treatment on the fatigue behavior and life of a disk. The whole numerical procedure is implemented in the framework of the finite element code ZSeT/ZeBuLoN. So the computation of the thermal evolution inside the part during the heat treatment, the resulting microstructure and the fatigue life analysis are performed with the same software. To illustrate this procedure, an example of multi-step computation is presented hereafter.

Firstly, the evolution of the temperature within a disk preform is simulated during a given heat treatment sequence. As an application, such calculations were performed for a disk preform cooled from 1200°C in a fluid characterized by a heat transfer coefficient of 1600 $W \cdot K^{-1} \cdot m^{-2}$ at 1200°C linearly decreasing to 800 $W \cdot K^{-1} \cdot m^{-2}$ at 25°C (Figure 9a). For instance, at point A, the computation gives a temperature of 975°C after one minute of cooling from 1200°C.

Then, the precipitation model [20, 21] is applied to determine the evolution of the microstructural parameters (size and volume fraction of the different populations of γ') during the cooling and the aging treatment. As for real engine parts, the disk is "machined" from the preform. The CRSS and the resulting plastic threshold are derived (equations 6 and 7) from the microstructural parameters obtained for the given heat treatment (Figure 9b) at each Gauss point of the disk mesh (Figure 9c).

A typical mechanical loading sustained by the disk during service life is simulated to account for the stress redistributions due to cyclic plasticity. For this inelastic analysis a specific elasto-viscoplastic constitutive model is applied for which the plastic threshold depends on the microstructural parameters [22]. The strain and stress amplitudes and the mean stress at the stabilized cycle are finally used to compute the fatigue life at 450°C. For this analysis, the SWT fatigue criterion is extended to multiaxial loading [22]. This calculation was carried out on a 540 mm diameter disk subjected to fatigue cycles by varying the rotational speed between 50 and 27500 rpm. The duration of the triangular cycle is 90 seconds. In the present case, the computed fatigue life is 37000 cycles and the critical point is located in the bore (Figure 9d).

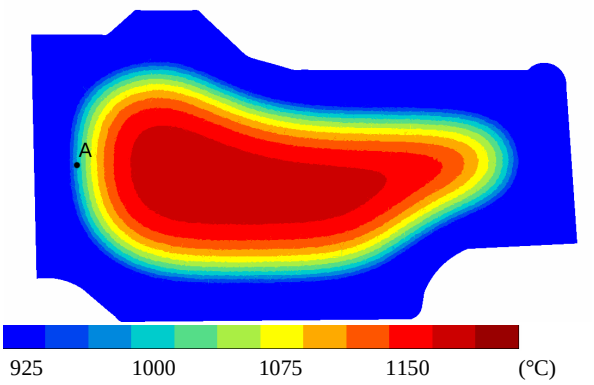

a) Temperature in a disk preform after one minute of cooling

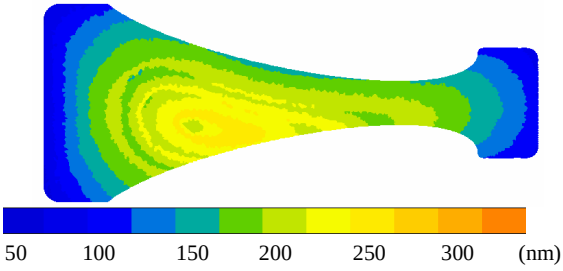

b) Mean radius of γ'_{II} precipitates in a disk after cooling

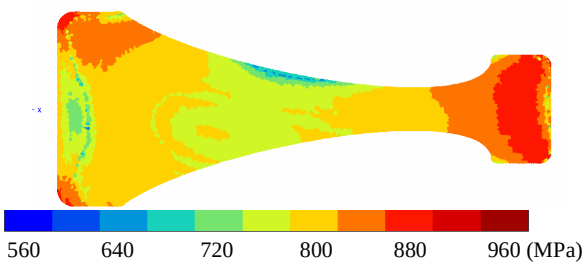

c) Plastic threshold stress in a disk after cooling

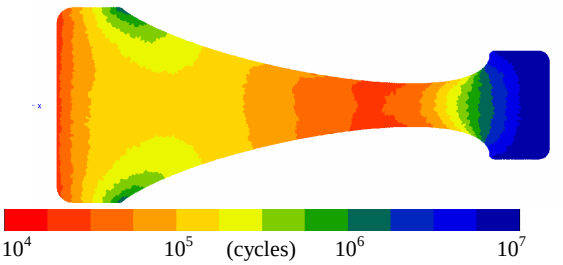

d) Fatigue life (90s triangular cycle between 50 and 27500 rpm)

Figure 9. Maps of the different steps of disk calculation from the heat treatment to fatigue life at 450°C
(half cross-section, the rotation axis on the left).

Table IV. 450°C experimental and calculated 0.2% yield stresses from experimental and precipitation model microstructure parameters for supersolvus N18 with various microstructures

Microstructure	"reference"		"no γ'_{III}"		"fine γ'_{II}"	
	Exp.	Model (250°C/min)	Exp.	Model (250°C/min)	Exp.	Model (700°C/min)
γ'_{II} fraction	0.46	0.485	0.47	0.50	0.40	0.47
γ'_{II} mean radius (nm)	102	125	108	128	70	77
γ'_{III} fraction	0.01	0.016	0	0	0.04	0.027
γ'_{III} mean radius (nm)	12.5	17	0	0	12.5	9
CRSS (eq 6) (MPa)	401	389	364	355	448	448
0.2%YS (eq 7) (MPa)	1042	1018	968	950	1136	1136
Experimental 0.2%YS (MPa)	1048		975		1135	

For a supersolvus heat treatment with a slower cooling (in a fluid characterized by a heat transfer coefficient of 200 $W \cdot K^{-1} \cdot m^{-2}$ at 1200°C linearly decreasing to 100 $W \cdot K^{-1} \cdot m^{-2}$ at 25°C), the calculated temperature at point A is 1175°C after one minute of cooling from 1200°C (location as in Figure 9a). The same computation procedure predicts a fatigue life of 69000 cycles and a critical point located in the web. These differences are mainly due to the effect of mean stress, which is higher in the case of the fast cooling condition.

This numerical modeling could be also an efficient tool for heat treatment optimization to improve other microstructure-dependent mechanical properties such as creep resistance.

Conclusions

The influence of γ' precipitate size and distribution was examined at 450°C on the tensile and LCF behaviors for powder metallurgy disk superalloy N18. Four γ' precipitate distributions were obtained through various cooling paths and/or aging treatments with a coarse grain size comparable for all heat treatments. It can be concluded from this investigation that:

- the γ' precipitation has no or little influence on the elastic and hardening moduli as well as on the cyclic hardening.
- The intragranular microstructure mainly affects 0.2%YS and UTS. 0.2%YS has an influence on the mean stress under non symmetrical loading but the resulting mean stress variations lead to limited effects on the fatigue life at 450°C.
- The fatigue law of coarse grain N18 is independent of the intragranular microstructure as long as the mean stress effect is correctly taken into account in the fatigue law.
- As expected for the coarse grain N18, analysis of fracture surfaces indicates that cracks initiate at large crystallographic facets and not at pores or ceramic inclusions.
- The coupling of a precipitation model with a CRSS calculation provides a good estimate of the 0.2%YS value from a given heat treatment sequence.
- A calculation loop is proposed enabling the optimization of heat treatment on disk preform to improve the fatigue life of a disk.

Acknowledgements

This work was supported by the French Ministry of Defence. The authors would like to express their thanks to J.-Y. Guédou and J.-M. Franchet from Safran Snecma for the material supply and their technical support. They would also like to acknowledge Ms C. Ramusat and Mr C. Rouaud for their assistance in this study.

References

1. J. Gayda, T.P. Gabb and P.T. Kantzos, "The effect of dual microstructure heat treatment on an advanced nickel-base disk alloy," *Superalloys 2004*, ed. K.A. Green *et al.* (Warrendale, PA, USA: TMS, 2004), 323-329.

2. T.P. Gabb, J. Gayda, J. Telesman and P.T. Kantzos, "Thermal and mechanical property characterization of the advanced disk alloy LSHR" (Report NASA TM-2005-213645, NASA, 2005).

3. J. Gayda, P.T. Kantzos and J. Telesman, "The effect of heat treatment on the fatigue behavior of Alloy 10" (Report NASA TM-2003-212473, NASA, 2003).

4. J.H. Moll and J.J. Conway, "Characteristics and properties of as-HIP P/M Alloy 720," *Superalloys 2000*, ed. T.M. Pollock *et al.* (Warrendale, PA, USA: TMS, 2000), 135-142.

5. J. Albrecht, "Comparing fatigue behavior of titanium and nickel-based alloys," *Mater Sci Eng*, A263 (1999), 176-186.

6. K.R. Bain, M.L. Gambone, J.M. Hyzak and M.C. Thomas, "Development of damage tolerant microstructures in Udimet 720" *Superalloys 1988*, ed. S. Reichman *et al.* (Warrendale, PA, USA: TMS, 1988), 13-22.

7. F. Alexandre, S. Deyber and A. Pineau, "Modelling the optimum grain size on the low cycle fatigue life of a Ni based superalloy in the presence of two possible crack initiation sites," *Scripta Mater*, 50 (2004), 25-30.

8. J.C. Runkle and R.M. Pelloux, "Micromechanisms of low-cycle fatigue in nickel-based superalloys at elevated temperatures" Fatigue Mechanisms ASTM-NBS-NSF Symposium, ed. J.T. Fong (ASTM, USA, 1979), 501-527.

9. H. Hattori, M. Takekawa, D. Furrer and R.J. Noel, "Evaluation of P/M U720 for gas turbine engine disk application," *Superalloys 1996*, ed. R.D. Kissinger *et al.* (Warrendale, PA, USA: TMS, 1996), 705-711.

10. R.J. Mitchell, J.A. Lemsky, R. Ramanathan, H.Y. Li, K.M. Perkins and L.D. Connor, "Process development & microstructure & mechanical property evaluation of a dual microstructure heat treated advanced nickel disc alloy," *Superalloys 2008*, ed. R.C. Reed *et al.* (Warrendale, PA, USA: TMS, 2008), 347-356.

11. S. Bashir and S.D. Antolovich, "The effect of microstructure, temperature, and hold-time on low-cycle fatigue of As-HIP P/M René 95" *Superalloys 1984*, ed. M. Gell *et al.* (Warrendale, PA, USA: TMS, 1984), 295-307.

12. M. Shenoy, J. Zhang and D.L. McDowell, "Estimating fatigue sensitivity to polycrystalline Ni-base superalloy microstructures using a computational approach," *Fatigue Fract Engng Mater Struct*, 30 (2007), 889-904.

13. B. Flageolet, "Effet du vieillissement du superalliage base nickel N18 pour disques de turbines sur sa durabilité en fatigue et en fatigue fluage à 700°C" (Ph.D. thesis, Université de Poitiers, France, 2005).

14. K.O. Findley and A. Saxena, "Low cycle fatigue in Rene 88DT at 650°C: crack nucleation mechanisms and modeling," *Met Mater Trans*, 37A (2006), 1469-1475.

15. T.P. Gabb, J. Telesman, P.T. Kantzos, P.J. Bonacuse and R.L. Barrie, "Initial assessment of the effects of nonmetallic inclusions on fatigue life of powder-metallurgy-processed Udimet® 720" (Report NASA TM-2002-211571, NASA, 2002).

16. T.P. Gabb, P.J. Bonacuse, L.J. Ghosn, J.W. Sweeney, A. Chatterjee and K.A. Green, "Assessments of low cycle fatigue behavior of powder metallurgy alloy U720" Fatigue and Fracture Mechanisms ASTM STP 1389, ed. G.R. Halford & J.P. Gallagher (ASTM, USA, 2000), 110-127.

17. J.-Y. Guédou, J.-C. Lautridou and Y. Honnorat, "N18, PM superalloy for disks: development and applications" *Superalloys 1992*, ed. S.D. Antolovich *et al.* (Warrendale, PA, USA: TMS, 1992), 267-276.

18. S.T. Wlodek, M. Kelly and D. Alden, "The structure of N18" *Superalloys 1992*, ed. S.D. Antolovich *et al.* (Warrendale, PA, USA: TMS, 1992), 467-476.

19. H. Loyer Danflou, M. Macia, T.H. Sanders and T. Khan "Mechanims of formation of serrated grain boundaries in nickel base superalloys" *Superalloys 1996*, ed. R.D. Kissinger *et al.* (Warrendale, PA, USA: TMS, 1996), 119-127.

20. G. Boittin, F. Gallerneau, D. Locq, P. Kanouté and G. Cailletaud, "Numerical modelling of the microstructure effect on fatigue behaviour of Ni-base superalloys for turbine disk, " *Technische Mechanik*, 30 (2010), 15-28.

21. N. Milhet-Gayraud, "Etude expérimentale et modélisation de la précipitation γ' dans le superalliage N18" (Ph.D. thesis, Institut National Polytechnique de Grenoble, France, 1994).

22. G. Boittin, "Expérimentation numérique pour l'aide à la spécification de la microstructure et des propriétés mécaniques d'un superalliage base Ni pour des applications moteur" (Ph.D. thesis, Mines-ParisTech, France, 2011).

23. J.-Y. Guédou, I. Augustins-Lecallier, L. Nazé, P. Caron and D. Locq, "Development of a new fatigue and creep resistant PM nickel-base superalloy for disk applications" *Superalloys 2008*, ed. R.C. Reed *et al.* (Warrendale, PA, USA: TMS, 2008), 21-30.

24. U.S. Department of Defense, Military Handbook - MIL-HDBK-5H: Metallic Materials and Elements for Aerospace Vehicle Structures, Knovel Interactive Edition, http://www.knovel.com/web/portal/basic_search/display?EXT KNOVEL DISPLAY bookid=754, 2003.

25. K.N. Smith, P. Watson and T.H. Topper, "A stress-strain function for the fatigue of metals," *J Mater*, 5 (1970), 767-778.

26. W. Hüther and B. Reppich, "Interaction of dislocations with coherent, stress-free, ordered particles", *Z Metallkd*, 69 (1978), 628-634.

27. L. Brown and R. Ham, *Dislocation-Particle Interactions*, in: Strengthening Methods in Crystals, ed. A. Kelly and R. Nicholson (Amsterdam, NL: Elsevier, 1971), 9-135.

28. B. Reppich, "Some new aspects concerning particle hardening mechanisms in γ' precipitating Ni-base alloys – I. Theoretical concept", *Acta Metall*, 30 (1982), 87-94.

29. M. Heilmaier, U. Leetz and B. Reppich, "Order strengthening in the cast nickel-based superalloy IN 100 at room temperature", *Mater Sci & Eng*, A319-321 (2001), 375-378.

30. Y.S. Choi, D.M. Dimiduk, M.D. Uchic and T.A. Parthasarathy, "A crystallographic constitutive model for Ni_3Al ($L1_2$) intermetallics", *Mater Sci & Eng*, A400-401 (2005), 256-259.

31. E. Nembach and G. Neite, "Precipitation hardening of superalloys by ordered γ'-particles", *Prog Mater Sci*, 29 (1985), 177-319.

32. L. Espié, "Etude expérimentale et modélisation numérique du comportement mécanique de monocristaux de superalliages" (Ph.D. thesis, Ecole Nationale Supérieure des Mines de Paris, France, 1996).